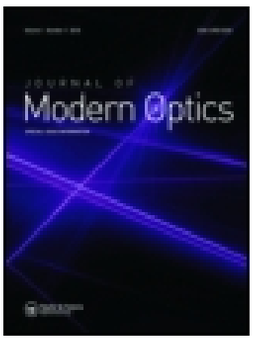

Journal of Modern Optics

ISSN: 0950-0340 (Print) 1362-3044 (Online) Journal homepage: https://www.tandfonline.com/loi/tmop20

Fringe visibility analysis with different scale apertures in speckle photography

Luciano Angel , Myrian Tebaldi , Marcelo Trivi & Néstor Bolognini

To cite this article: Luciano Angel , Myrian Tebaldi , Marcelo Trivi & Néstor Bolognini (2001) Fringe visibility analysis with different scale apertures in speckle photography, Journal of Modern Optics, 48:11, 1749-1765, DOI: 10.1080/09500340108231431

To link to this article: https://doi.org/10.1080/09500340108231431

JOURNAL OF MODERN OPTICS, 2001, VOL. 48, NO. 11, 1749–1765

Fringe visibility analysis with different scale apertures in speckle photography

LUCIANO ANGEL

Departamento de Ciencias Básicas, Universidad EAFIT, P.O. Box. 3300, Medellín, Colombia

MYRIAN TEBALDI, MARCELO TRIVI, NÉSTOR BOLOGNINI

Centro de Investigaciones Ópticas, CIOp (CONICET, CIC) and OPTIMO (Dpto. de Fisicomatemática, Facultad de Ingeniería, UNLP), P.O. Box 124, (1900), La Plata, Argentina; e-mail: Nestorb@odin.ciop.unlp.edu.ar

(*Received 4 December 2000; final version received 18 April 2001*)

Abstract. The use of different scale aperture pupils for image recording in speckle photography is analysed. In particular a double-exposure specklegram is considered. The ensemble-average intensity in the Fourier plane is analytically derived and fringe visibility is investigated. The theoretical results are verified by in-plane displacement translation experiments.

1. Introduction

It is well known that when an optically rough surface is illuminated by coherent light, speckles appear in front of the surface. Rigid body movements and deformation experimented by the input surface are responsible for displacements and structural changes observed in speckles, which can be analysed on the basis of double-exposing imaged speckles, before and after deformation. In particular, the speckle photography technique allows one to determine in plane displacement deformation, vibration and tilt of diffusely reflecting surfaces. The speckle displacement caused by object displacement or deformation is detected by means of coherent processing of the double exposed specklegram and it is derived, for example, from the Young fringes that are obtained by optical Fourier transforming of the specklegram. The speckle photography technique was investigated by Burch and Tokarski [1], Archbold, Burch and Ennos [2], Archbold and Ennos [3], Kethan and Chiang [4] and Yamaguchi [5, 6].

When double exposing, each of the speckle distributions fields have a correlation area corresponding to the mean size of speckles and the object displacement between exposures gives rise to a displacement and a decorrelation between speckles. The speckle displacement and the speckle structure changes have been investigated by calculating the cross-correlation speckle function intensities, before and after displacement. The dependencies of speckle correlation properties

Journal of Modern Optics ISSN 0950–0340 print/ISSN 1362–3044 online © 2001 Taylor & Francis Ltd
http://www.tandf.co.uk/journals
DOI: 10.1080/09500340110062261

on the object illumination textures as well as on the displacement parameters have previously been theoretically analysed [5 ,7 ,8].

To measure accurately the periodicity of the Young's fringes obtained in speckle photography, the intensity profile of the diffraction halo was analysed [9, 10]. In an image configuration, the form of the diffraction halo is determined by the aperture function of the recording lens. If the intensity distribution of the imaged speckle pattern is uniform, ergodic and Gaussian, then the diffraction halo is equal to the power spectrum of the image-plane speckle intensity [10].

In a previous paper the use of different multiple aperture pupils for recording each image in speckle photography was analysed [11]. The introduction of suitable spatial frequency carriers, by internally modulating imaged speckles, allows one to isolate or combine selectively the spectral content of different images into spatially separated regions in the Fourier plane.

In [11], by considering a different multiple aperture pupil in each exposure, the ensemble-average intensity in the Fourier plane is analytically derived and fringe visibility is investigated. The apertures all have the same shape and scale but the number and location of the apertures can be modified between exposures.

To generalize previous analysis, in this paper we study the use of different scale aperture pupils for recording each image in speckle photography. We consider a scale factor associated to each coordinate axis of the pupils. On this basis, the decorrelation introduced by the change of the pupil aperture scale between exposures is analysed. However, we do not consider the decorrelation introduced as a consequence of the object displacement or changes in the illumination conditions.

In section 3.1, we analyse the simple case of employing one circular aperture whose scale is modified between exposures. Later, in section 3.2, we consider the use of a pair of square apertures in the first exposure, which are replaced by a pair of rectangular apertures in the second exposure. In both cases, the cross-correlation functions of speckle amplitudes and intensities in the image plane are evaluated, in terms of the geometric characteristics of the pupils. Then, the intensity in the Fourier plane and the fringe visibility is experimentally and theoretically analysed.

2. Theoretical analysis

Let us consider the experimental set-up of figure 1. In figure 1 (*a*) the recording arrangement is depicted. A random diffuser, located at the input plane x–y, is illuminated by means of a collimated laser beam of wavelength λ_W. This beam impinges perpendicularly to the mean (or smoothed) diffuser surface.

An image of this input is formed in the X–Y plane, by using a lens L_1 located at the u–v plane. Besides, to image the input $A_0^k(x, y)$, a pupil mask $P^k(u, v)$ is placed immediately in front of the lens. This function $P^k(u, v)$ is unity inside the apertures and zero otherwise.

The analysis procedure of the specklegram is shown in figure 1 (*b*). In this case, a collimated laser beam of wavelength λ_R illuminates the specklegram positioned in the X–Y plane. In order to give a general treatment, we consider different wavelengths in the read-out and reconstruction processes. Afterwards, the transmitted light is Fourier transformed by means of a lens L_2 of focal length f and the intensity distribution is observed at the U–V focal plane.

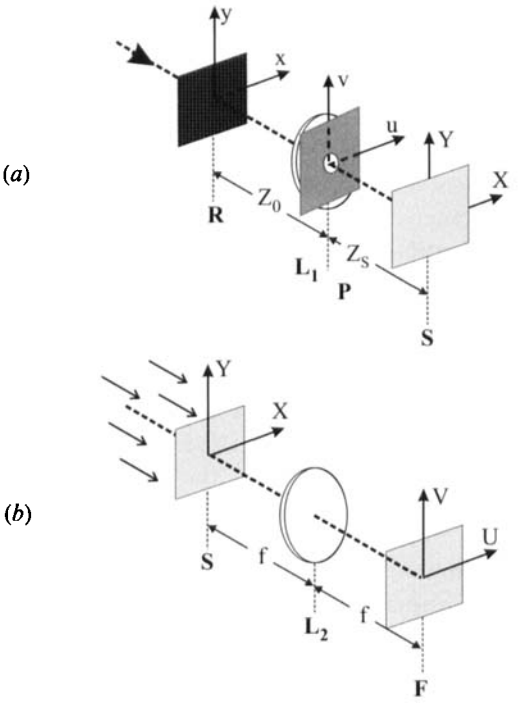

Figure 1. Experimental set-up: (*a*) recording and (*b*) analysis of the specklegram. R: diffuser: L_1: imaging lens, P: pupil mask: S: specklegram; L_2: Fourier lens, F: Fourier plane.

In [11] a multiple exposure was analysed by using different pupil arrangements between exposures and it was demonstrated that the average intensity in the Fourier plane results:

$$\langle I_f(U,V)\rangle = \sum_{k=1}^{N} \Im\{|\Im\{P^k(u,v)\}(X,Y)|^2\}(\vartheta U, \vartheta V) + 2\sum_{\substack{k,l=1\\(k<l)}}^{N} \cos\left(\frac{2\pi}{\lambda_R f}[U\,\Delta X^{kl} + V\,\Delta Y^{kl}]\right) \times \Im\{|\Im\{P^{kl}(u,v)\}(X,Y)|^2\}(\vartheta U, \vartheta V). \quad (1)$$

In this equation, the smoothed function

$$\Im\{|\Im\{P^k(u,v)\}(X,Y)|^2\}(\vartheta U, \vartheta V) \approx \int |P^k(\xi,\eta)|^2 |P^k(\xi - \vartheta U, \eta - \vartheta V)|^2 \,\mathrm{d}\xi\,\mathrm{d}\eta \quad (2)$$

represents the diffraction halo corresponding to the pupil P^k [10, 12], $\vartheta = (\lambda_W Z_C/\lambda_R f)$, Z_0 and Z_C are the distances from the diffuser to the lens and from the lens to the image plane, respectively. $\Im$ denotes a two-dimensional Fourier transform.

Furthermore, by considering that $A^k(X,Y)$ and $A^l(X,Y)$ represent the image amplitude fields belonging to different positions of the diffuser and $(\Delta x^{kl}, \Delta y^{kl})$

stands for the relative uniform in-plane displacement the diffuser undergoes between registered images, then:

$$(\Delta X^{kl}, \Delta Y^{kl}) = -\frac{Z_C}{Z_0}(\Delta x^{kl}, \Delta y^{kl}) \tag{3}$$

is the relative displacement of $A^l(X, Y)$ with respect to $A^k(X, Y)$. It was assumed that the speckle displacement takes place near the optical axis.

The first term in equation (1) describes the overlapping of all the smoothed diffraction halos, each one corresponding to an individual single-exposure recording $\Im\{|\Im\{P^k\}|^2\}$. Note that this term does not contribute to fringes formation. Each pair of pupils $P^k(u, v)$ and $P^l(u, v)$ can be associated to an independent contribution to fringe formation, related exclusively with the common part $P^{kl}(u, v) = P^k(u, v)[P^l(u, v)]^*$ of both pupils and the relative displacement of the respective images. Similarly, the factor $\Im\{|\Im\{P^{kl}\}|^2\}$ in the second term of equation (1) can be interpreted in terms of the halos associated with P^{kl}, which are fringe modulated. Specifically, spatial frequencies corresponding to a relative displacement $(\Delta K^{kl}, \Delta Y^{kl})$ are observed at the loci of the diffraction halo of P^{kl}. Nevertheless, if the common part of the pupils is null ($P^{kl}(u, v) = 0$), then no fringe formation can be associated with the kth and the lth recorded images. In summary, the second term of equation (1) stands for a rather complex pattern, which results from the selective overlapping of elemental fringe modulated diffraction spots.

Now, in this paper our interest is to analyse the effect of changing the pupil aperture scale. Then, we consider two images recorded by using pupils satisfying the conditions

$$P^1(u, v) = \sum_{j=1}^{q} a(u - u_j, v - v_j), \tag{4}$$

$$P^2(u, v) = \sum_{j=1}^{q} a\left(\frac{u - u_j}{e_1}, \frac{v - v_j}{e_2}\right), \tag{5}$$

where e_1 and e_2 are positive constants which determine the scale change introduced in the respective axes, q is the number of apertures in the pupils and the aperture shape $a(u, v)$ is defined by the expression

$$a_j(u, v) = a(u - u_j, v - v_j) = \begin{cases} 1 & \text{inside the } j\text{th aperture of } P^1(u, v), \\ 0 & \text{otherwise,} \end{cases} \tag{6}$$

where (u_j, v_j) are constant vectors for $j = 1, 2, \ldots, q$. By comparing the diffraction patterns corresponding to any pair of the pupils to be employed, it is inferred that a region of the spots of one diffraction pattern coincides with a region of the diffraction spots of the other pattern.

By using equations (4), (5) and (6) it follows:

$$|\Im\{|P^2(u, v)|^2\}(X, Y)|^2 = (e_1 e_2)^2 |\Im\{a(u, v)\}(e_1 X, e_2 Y)|^2 \times \left\{ q + \sum_{\substack{k,l=1 \\ (k \neq l)}}^{q} \exp\left[i2\pi(u_{kl} X + v_{kl} Y)\right] \right\}, \tag{7}$$

where $(u_{kl}, v_{kl}) \equiv (u_l - u_k, v_l - v_k)$. Then, the Fourier transform of equation (7) results:

$$\Im\{|\Im\{|P^2(u,v)|^2\}(X,Y)|^2\}(\vartheta U, \vartheta V) = qa\left(-\frac{\vartheta U}{e_1}, -\frac{\vartheta V}{e_2}\right) * a\left(\frac{\vartheta U}{e_1}, \frac{\vartheta V}{e_2}\right) + \sum_{\substack{k,l=1 \\ (k\neq l)}}^{q} a\left(-\frac{\vartheta U - u_{kl}}{e_1}, -\frac{\vartheta V - v_{kl}}{e_2}\right) \times a\left(\frac{\vartheta U - u_{kl}}{e_1}, \frac{\vartheta V - v_{kl}}{e_2}\right). \tag{8}$$

In particular when $e_1 = e_2 = 1$,

$$\Im\{|\Im\{|P^1(u,v)|^2\}(X,Y)|^2\}(\vartheta U, \vartheta V) = qa(-\vartheta U, -\vartheta V) * a(\vartheta U, \vartheta V) + \sum_{\substack{k,l=1 \\ (k\neq l)}}^{q} a(-\vartheta U + u_{kl}, -\vartheta V + v_{kl}) \times a(\vartheta U - u_{kl}, \vartheta V - v_{kl}). \tag{9}$$

On the other hand, from equations (4) and (5):

$$P^{12}(u,v) \equiv P^1(u,v)[P^2(u,v)]^* = \sum_{j=1}^{q} a(u - u_j, v - v_j) a\left(\frac{u - u_j}{e_1}, \frac{v - v_j}{e_2}\right), = \sum_{j=1}^{q} a\left(\frac{u - u_j}{e_1'}, \frac{v - v_j}{e_2'}\right), \tag{10}$$

where:

$$e_1' = \min\{1, e_1\} = \begin{cases} 1 & \text{si} \quad e_1 \geqslant 1 \\ e_1 & \text{si} \quad e_1 < 1 \end{cases}$$

and

$$e_2' = \min\{1, e_2\} = \begin{cases} 1 & \text{si} \quad e_2 \geqslant 1 \\ e_2 & \text{si} \quad e_2 < 1. \end{cases}$$

In this case,

$$\Im\{|\Im\{P^{12}(u,v)\}(X,Y)|^2\}(\vartheta U, \vartheta V) = qa\left(-\frac{\vartheta U}{e_1'}, -\frac{\vartheta V}{e_2'}\right) * a\left(\frac{\vartheta U}{e_1'}, \frac{\vartheta V}{e_2'}\right) + \sum_{\substack{k,l=1 \\ (k\neq l)}}^{q} a\left(-\frac{\vartheta U - u_{kl}}{e_1'}, -\frac{\vartheta V - v_{kl}}{e_2'}\right) \times a\left(\frac{\vartheta U - u_{kl}}{e_1'}, \frac{\vartheta V - v_{kl}}{e_2'}\right). \tag{11}$$

By considering equations (8), (9) and (11), the average intensity in the Fourier plane given by equation (1) becomes:

$$\langle I_f(U,V)\rangle = \langle I_f^0(U,V)\rangle + \langle I_f^{+1}(U,V)\rangle + \langle I_f^{-1}(U,V)\rangle, \tag{12}$$

where:

$$\begin{aligned}\langle I_f^0(U,V)\rangle = CAI_{\mathrm{R}}q\Big\{ & a(-\vartheta U,-\vartheta V) * a(\vartheta U,\vartheta V)\\ & + a\left(-\frac{\vartheta U}{e_1},-\frac{\vartheta V}{e_2}\right) * a\left(\frac{\vartheta U}{e_1},\frac{\vartheta V}{e_2}\right)\\ & + 2\cos\left[\frac{2\pi}{\lambda_{\mathrm{R}} f}(U\Delta X^{12} + V\Delta Y^{12})\right] a\left(-\frac{\vartheta U}{e_1'},-\frac{\vartheta V}{e_2'}\right)\\ & \times a\left(\frac{\vartheta U}{e_1'},\frac{\vartheta V}{e_2'}\right)\Big\},\end{aligned} \tag{13}$$

$$\begin{aligned}\langle I_f^{\pm 1}(U,V)\rangle = CAI_{\mathrm{R}}q\sum_{\substack{k,l=1\\(k<l)}}^{q}\Big\{ & a(-\vartheta U \pm u_{kl},-\vartheta V \pm v_{kl}) * a(\vartheta U \mp u_{kl},\vartheta V \mp v_{kl})\\ & + a\left(\frac{-\vartheta U \pm u_{kl}}{e_1},\frac{-\vartheta V \pm v_{kl}}{e_2}\right) * a\left(\frac{\vartheta U \mp u_{kl}}{e_1},\frac{\vartheta V \mp v_{kl}}{e_2}\right)\\ & + 2\cos\left[\frac{2\pi}{\lambda_{\mathrm{R}} f}(U\Delta X^{12} + V\Delta Y^{12})\right] a\left(\frac{-\vartheta U \pm u_{kl}}{e_1'},\frac{-\vartheta V \pm v_{kl}}{e_2'}\right)\\ & \times a\left(\frac{\vartheta U \mp u_{kl}}{e_1'},\frac{\vartheta V \mp v_{kl}}{e_2'}\right)\Big\},\end{aligned} \tag{14}$$

where C is a constant value that depends on the recording parameters (distance Z_0 and Z_{C}, recording intensity, wavelength, etc.), the constant factor A represents the finite area of the specklegram and I_{R} is the read-out intensity.

This general result can be used in all cases when a double-exposure specklegram employs pupils with different scale for each exposure. In the case analysed, the diffraction patterns corresponding to any pair of pupils to be employed, the loci of the spots of one diffraction pattern partially coincide with a region of the diffraction spots of the other pattern.

Note that $\langle I_f^{\pm 1}(U,V)\rangle$ represents the average intensity distribution for the lateral diffraction spots and $\langle I_f^0(U,V)\rangle$ represents the zero order contribution in the Fourier plane. The first and second terms of equations (13) and (14) are not associated with fringe formation in the respective spots. Besides, the third term determines the contribution to fringes formation.

3. Experimental results

3.1. *Double-exposure specklegram with a single aperture scaled between exposures*

Each imaged speckle distribution was recorded by using the conventional arrangement shown in figure 1. As a first example, we consider a double exposure specklegram using the pupils $P^1(u,v)$ and $P^2(u,v)$. Each pupil has one circular aperture ($q = 1$) of diameter D_1 and D_2, respectively. The pupils are represented by:

$$P^k(u,v) = \mathrm{cyl}\left(\frac{r}{D_k}\right) = \begin{cases} 1 & \text{if} \quad 0 \leqslant r \leqslant D_k/2 \\ 0 & \text{if} \quad r > D_k/2 \end{cases} \qquad k = 1, 2, \tag{15}$$

where $r = \sqrt{u^2 + v^2}$. In our case, $e_1 = e_2 = D_2/D_1 \equiv e, e_1' = e_2' = 1$ and the apertures are concentric.

By using equations (12), (13), (14) and (15), the average intensity in the Fourier plane results:

$$\langle I_f U, V)\rangle = CAI_{\mathrm{R}}\left\{\aleph\left(\frac{\rho}{D_2'}\right) + \aleph\left(\frac{\rho}{D_1'}\right)\left[1 + 2\cos\left(\frac{2\pi}{\lambda_{\mathrm{R}} f}(U\Delta X^{12} + V\Delta Y^{12})\right)\right]\right\}, \tag{16}$$

where $\rho = \sqrt{U^2 + V^2}$, $D_k' = 2D_k\vartheta = 2D_k\lambda_{\mathrm{R}} f/\lambda_{\mathrm{W}} Z_{\mathrm{C}}$ and

$$\begin{aligned}\aleph\left(\frac{\rho}{D_k'}\right) &= P^k(-\vartheta U, -\vartheta V) * P^k(\vartheta U, \vartheta V) = \mathrm{cyl}\left(\frac{2\rho}{D_k'}\right) * \mathrm{cyl}\left(\frac{2\rho}{D_k'}\right) \\ &= \tfrac{1}{2} D_k^2 \,\mathrm{cyl}\left(\frac{\rho}{D_k'}\right)\left[\cos^{-1}\left(\frac{2\rho}{D_k'}\right) - \left(\frac{2\rho}{D_k'}\right)\left(1 - \left(\frac{2\rho}{D_k'}\right)^2\right)^{1/2}\right].\end{aligned} \tag{17}$$

The function $\aleph(\rho/D_k')$ stands for a (smoothed) circular diffraction spot of diameter D_k', associated with the pupil $P^k(u,v)$ centred at the origin of the U–V plane [10]. In consequence D_1' and D_2' represent the diameters of the halo of $P^1(u,v)$ and $P^2(u,v)$, respectively. From equation (16) it is apparent that the interference fringes are obtained only in the region corresponding to the halo of $P^1(u,v)$. In fact, for $\rho \geqslant D_1'/2$ the average intensity coincides with the diffraction of the second exposure. This behaviour is confirmed by observing figure 2.

Figure 2 (*a*) shows a 3-D display of the function $\langle I_f(U,V)\rangle$, that represents a double exposure specklegram obtained by apertures of different diameters (see equations (16) and (17)). Figure 2 (*b*) shows the intensity profile perpendicular to the interference fringes direction. There, the parameters values: $\lambda_{\mathrm{W}} = 514\,\mathrm{nm}$, $\lambda_{\mathrm{R}} = 633\,\mathrm{nm}$, $Z_{\mathrm{C}} = 485\,\mathrm{mm}$, $f = 100\,\mathrm{mm}$, $D_1 = 12\,\mathrm{mm}$, $D_2 = 20\,\mathrm{mm}$ and $\Delta X^{12} = 80\,\mu\mathrm{m}$ were employed. Note that to give a general result we use two different wavelengths for the recording and read-out processes.

Notice, from equation (16), that the average intensity modulation appears in the region existing between the envelopes:

$$\langle I_f(U,V)\rangle_{\max} = CAI_{\mathrm{R}}\left[\aleph\left(\frac{\rho}{D_2'}\right) + 3\aleph\left(\frac{\rho}{D_1'}\right)\right], \tag{18}$$

$$\langle I_f(U,V)\rangle_{\min} = CAI_{\mathrm{R}}\left[\aleph\left(\frac{\rho}{D_2'}\right) - \aleph\left(\frac{\rho}{D_1'}\right)\right]. \tag{19}$$

This fact can be confirmed by observing figure 2 (*b*): in this case for $\rho \geqslant D_1'/2$ both envelopes coincide and also coincide with the diffraction halo corresponding to the second exposure.

By using the intensity envelopes given by equations (18) and (19), the visibility of the interference fringes [9, 13] results:

$$\mathbf{V}(U,V) \equiv \frac{\langle I_f(U,V)\rangle_{\max} - \langle I_f(U,V)\rangle_{\min}}{\langle I_f(U,V)\rangle_{\max} + \langle I_f(U,V)\rangle_{\min}} = \frac{2\aleph(\rho/D_1')}{\aleph(\rho/D_1') + \aleph(\rho/D_2')}. \tag{20}$$

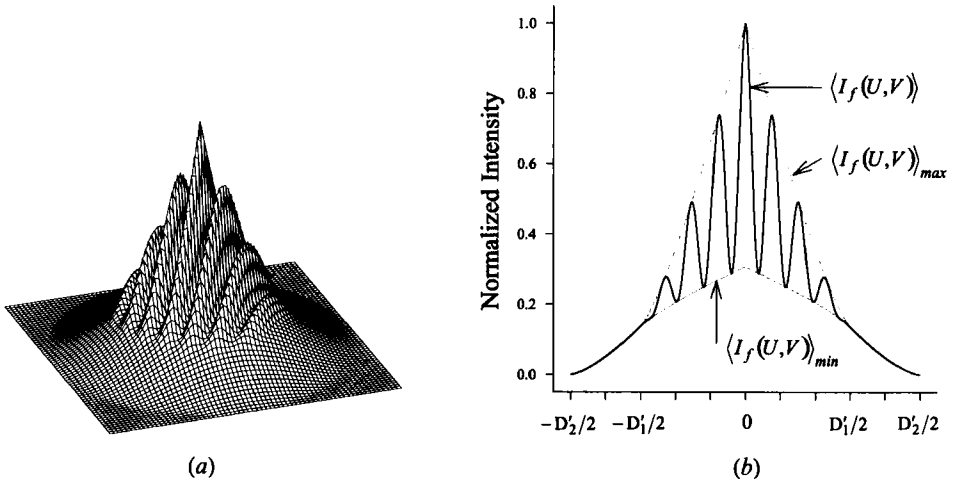

Figure 2. Theoretical simulation of the average intensity in the Fourier plane: (*a*) 3D representation; (*b*) line profile along a line perpendicular to the fringe direction.

Figure 3 depicts the visibility behaviour versus the distance to the Fourier plane origin, for different values of the scale parameter $e = D_2/D_1$. Note that in the origin ($\rho = 0$) the visibility is maximum and result $\mathbf{V}(0) = 2(1+e^2)^{-1}$. By increasing ρ the visibility decrease. Also, for $\rho \geqslant D_1'/2$ the visibility is null.

It should be pointed out that the fringe visibility is determined by the correlation properties of the image field, which depend on the scale factor value e.

In our case, $|P^2(u,v)|^2 = P^2(u,v) = \mathrm{cyl}\,(r/D_2)$ and $P^{12}(u,v) = |P^1(u,v)|^2 = P^1(u,v) = \mathrm{cyl}\,(r/D_1)$. Also

$$\Im\left\{\mathrm{cyl}\left(\frac{r}{D_k}\right)\right\}(\chi,\eta) = \frac{\pi}{4}D_k^2\,\mathrm{somb}\,(D_k\rho) \tag{21}$$

where $\rho = \sqrt{\chi^2+\eta^2}$ and $\mathrm{somb}\,(D_k\rho) = 2J_1(\pi D_k\rho)/\pi D_k\rho$, where J_1 is the first class and first-order Bessel function. Under this condition and by using the cross-correlation function of the image amplitudes and the average intensity in the image plane obtained in [11], the modulus of the normalized amplitude correlation function results:

$$|\mu^{12}| \equiv \frac{|\langle A^1(X_a, Y_a)[A^2(X_b, Y_b)]^*\rangle|}{[\langle I^1\rangle\langle I^2\rangle]^{1/2}} = e^{-1}|\,\mathrm{somb}\,(D_1\sqrt{\chi^2+\eta^2})| \tag{22}$$

for

$$(\chi,\eta) = \left(\frac{X_a - X_b}{\lambda_W Z_C} - \frac{\Delta x^{12}}{\lambda_W Z_0}, \frac{Y_a - Y_b}{\lambda_W Z_C} - \frac{\Delta y^{12}}{\lambda_W Z_0}\right).$$

The factor $|\mu^{12}|$ depends on the diffuser displacement and of the coordinates (X_a, Y_a) and (X_b, Y_b). But to analyse the decorrelation effect introduced only by the pupil change, we evaluate $|\mu^{12}|$ for a null displacement and in the same point of the image plane. In this case, by replacing $(\chi,\eta) = 0$ in equation (22), we obtain $|\mu^{12}| = e^{-1}$, that is the maximum value of the amplitude correlation function.

It should be noted that e^{-1} does not represent only the rate between the aperture diameters. It represents the relation between the average speckle trans-

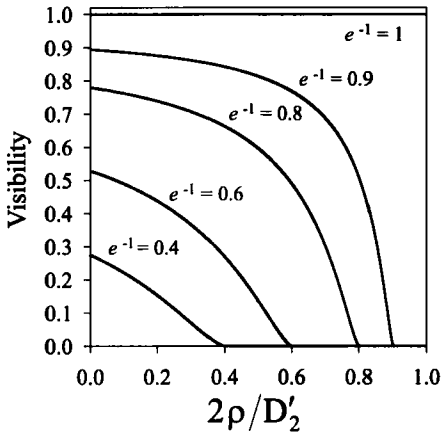

Figure 3. Fringe visibility curves for different values of the parameter e^{-1} obtained by using scaled circular aperture pupils.

versal dimensions of the respective speckles. The average diameter of the speckle image is given by $\delta t_k \approx (1.2)\lambda_W Z_C/D_k (k = 1, 2)$, which decreases in the same proportion as the aperture diameter increases [14]. Then, in our case the speckle diameter corresponding to the second register is e times smaller than in the first exposure. Also, the average intensity at the image plane decreases in proportion as the aperture area, because the area limits the energy passing through the pupil in each case. This feature can be visualized in figure 4, which shows four speckle patterns corresponding to the pupil diameters (*a*) $D = 8$ mm, (*b*) $D = 12$ mm, (*c*) $D = 16$ mm and (*d*) $D = 20$ mm. The images are recorded by the set-up of figure 1 and by using a CCD camera, with a zoom-microscope providing a lateral magnification of 4.5× and focused on the observation X–Y plane. The parameters employed are $Z_0 = 135$ mm and $Z_C = 485$ mm. $\lambda_W = 633$ nm. The average diameter of the imaged speckles shown in figure 4 are: $\delta t \approx 46.1$ μm in (*a*), 30.7 μm in (*b*), 23.0 μm in (*c*) and 18.4 μm in (*d*).

Figure 5 displays the diffraction pattern intensity distribution corresponding to a double exposure specklegram obtained in the Fourier plane for different values of the pupil scale factor e. In this case, the set-up of figure 1 is used for recording and reading out processes. As recording material, a holographic film (Agfa-Gevaert 10E-75) is used and for recording and read-out process a He–Ne Laser ($\lambda_W = \lambda_R = 633$ nm) is employed. In this case, the parameters are: $Z_C = 485$ mm, $Z_0 = 135$ mm and $f = 100$ mm, $\Delta x^{12} = 40$ μm. In the first exposure the pupil diameter is $D_2 = 20$ mm in all cases and in the second exposure the corresponding diameters are: (*a*) $D_1 = 20$ mm, (*b*) $D_1 = 16$ mm, (*c*) $D_1 = 12$ mm and (*d*) $D_1 = 8$ mm, respectively. Then, the scale parameter $e = D_2/D_1$ gives (*a*) $e = 1$, (*b*) $e = 1.25$, (*c*) $e = 1.67$ and (*d*) $e = 2.5$, respectively.

In the images of figure 5 the external diffraction halo area (associated to the second exposure) is the same in all images because the pupil area is the same in all cases. Nevertheless, the area of the fringes modulating images is different in each image because this area is proportional to the pupil area employed in the first exposure. Note that the fringe visibility decreases when the parameter e defined as the pupil diameter ratio increases. The best fringe visibility is observed in figure 5

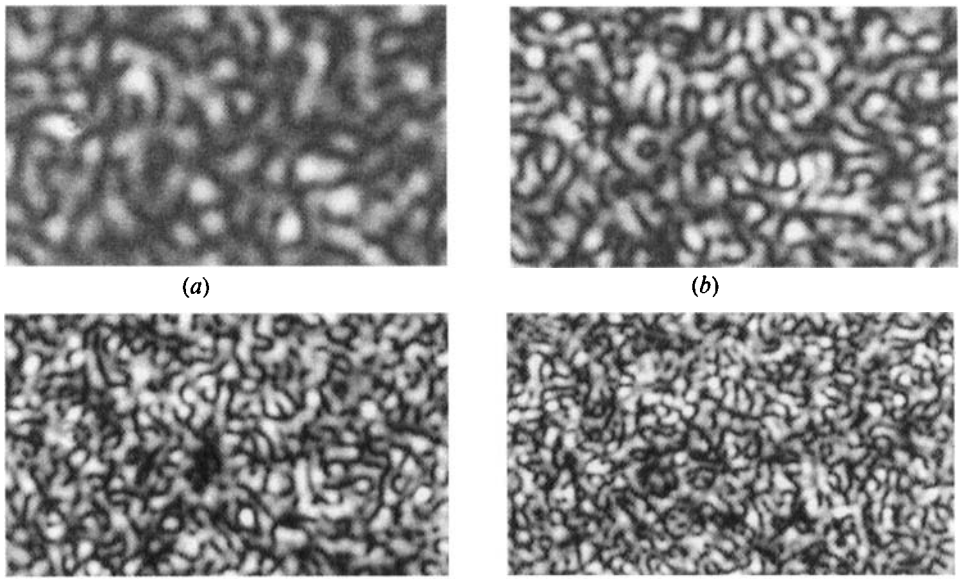

(*a*) (*b*)

(*c*) (*d*)

Figure 4. Speckle intensity distribution in the image plane by using in each exposure circular apertures with different diameter (*a*) $D = 8\,\text{mm}$; (*b*) $D = 12\,\text{mm}$; (*c*) $D = 16\,\text{mm}$; and (*d*) $D = 20\,\text{mm}$.

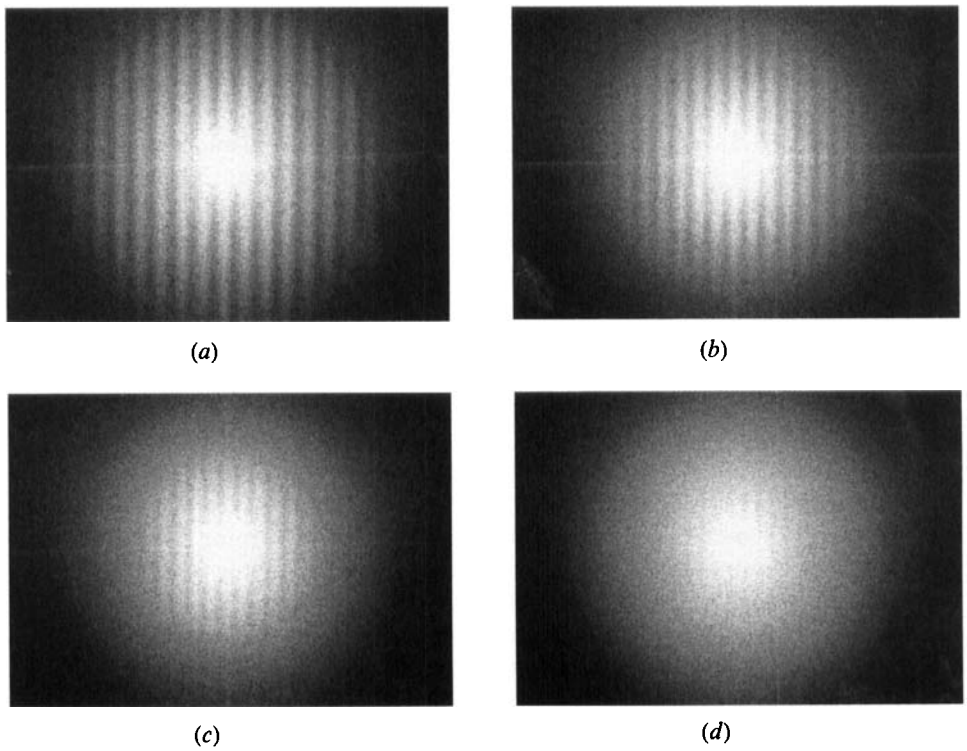

(*a*) (*b*)

(*c*) (*d*)

Figure 5. Double-exposure specklegrams by using a single circular aperture pupil with the following scale factors (*a*) $e = 1$, (*b*) $e = 1.25$, (*c*) $e = 1.67$, and (*d*) $e = 2.5$.

(*a*) because, in this case, the two pupil scales coincide and in consequence the speckle patterns are fully correlated.

3.2. *Double-exposure specklegram by two-apertures scaled between exposures*

In this section, the double-exposure specklegram using a pupil mask with two apertures ($q = 2$) whose scale is modified between exposures is considered. The first exposure pupil has two square apertures of D mm side and the second exposure pupil consists of rectangular apertures of area $e_1 D \times e_2 D (e_1 = 1, e_2 \equiv e > 1)$ (see figure 6). Then, the pupils can be represented by:

$$P^1(u,v) = \left[\text{rect}\left(\frac{u}{D}\right) + \text{rect}\left(\frac{u-d}{D}\right)\right]\text{rect}\left(\frac{v}{D}\right), \tag{23}$$

$$P^2(u,v) = \left[\text{rect}\left(\frac{u}{D}\right) + \text{rect}\left(\frac{u-d}{D}\right)\right]\text{rect}\left(\frac{v}{eD}\right), \tag{24}$$

where d defines the distance between the aperture centres. It is clear that $u_{12} = d$ and $v_{12} = 0$.

Taking into account the aperture scale change, the speckle average transversal dimension is e times reduced in the vertical axis at the second exposure with respect to the first one, as can be observed in figure 6. For these images the parameters are: $\lambda_W = 633\,\text{nm}$, $Z_C = 485\,\text{mm}$, $Z_0 = 135\,\text{mm}$, $d = 10\,\text{mm}$, $D = 3.8\,\text{mm}$ and $e = 2$. Then, the vertical lengths are $96.9\,\mu\text{m}$ and $48.5\,\mu\text{m}$ in the first and second exposure, respectively, and the horizontal dimensions are not modified.

By using a pupil mask with two apertures, a speckled image of the input is produced through each aperture. The complex amplitudes of waves passing through different apertures are statistically independent from each other since different components of the angular spectrum of scattered light are accepted by the apertures. Thus, the speckle image distribution formed through one aperture is uncorrelated with the distribution obtained through another one. Moreover, the resulting speckle pattern appears as the interference of the mentioned distributions because they are coherent. Let us consider a pair of spatially coincident speckle grains. Their phases are constant and they are coherent. Then, these grains are fringe modulated and the fringes are perpendicular to the line joining the points (u_n, v_n) and (u_m, v_m) that defines the aperture centres. Besides, the fringes of the elemental fringe system form an angle $\alpha_{nm} = \tan^{-1}[(v_m - v_n)/(u_m - u_n)]$ with the X axis. The average spatial period of the fringes is $\Lambda = Z_C \lambda_W / d'$ where d' represents the mean separation between the respective apertures. In our case, the average spatial period is $30.7\,\mu\text{m}$. It is apparent that the orientation of fringes is approximately perpendicular to the line joining the centres of the respective apertures. However, as can be confirmed by observing figure 6, the period, orientation and phase of the fringe system modulating the individual speckles vary slightly from one speckle to another.

Then, we evaluate the average intensity in the Fourier plane for the double exposure specklegram by using two apertures as described above, whose scale is modified between exposures. From equations (12), (13) and (14):

$$\langle I_f(U,V)\rangle = \langle I_f^0(U,V)\rangle + \langle I_f^{+1}(U,V)\rangle + \langle I_f^{-1}(U,V)\rangle, \tag{25}$$

where:

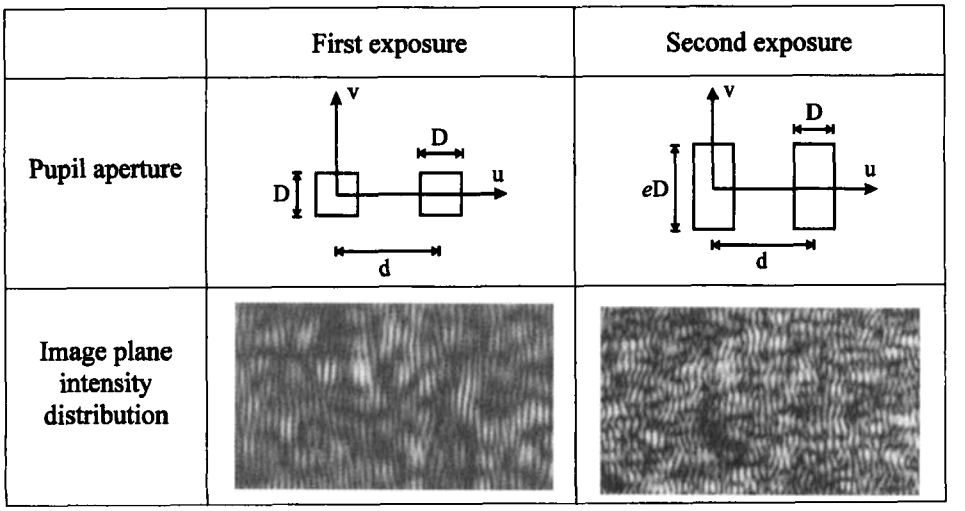

Figure 6. First row shows the pupil aperture corresponding to the first exposure and second exposure, respectively. The second row shows the speckle intensity distribution in the image plane obtained through the pupil apertures schematized in the first row.

$$\langle I_f^0(U,V)\rangle = CAI_R D^2\, 2\,\mathrm{trian}\left(\frac{2U}{D'}\right)\left\{e\,\mathrm{trian}\left(\frac{2V}{eD'}\right) + \mathrm{trian}\left(\frac{2V}{D'}\right)\left[1+2\cos\left(\frac{2\pi}{\lambda_R f}(U\Delta X^{12}+V\Delta Y^{12})\right)\right]\right\}, \quad (26)$$

$$\langle I_f^{\pm 1}(U,V)\rangle = CAI_R D^2\,\mathrm{trian}\left(\frac{2}{D'}(U\mp \mathrm{d}')\right)\left\{e\,\mathrm{trian}\left(\frac{2V}{eD'}\right) + \mathrm{trian}\left(\frac{2V}{D'}\right)\left[1+2\cos\left(\frac{2\pi}{\lambda_R f}(U\Delta X^{12}+V\Delta Y^{12})\right)\right]\right\}, \quad (27)$$

$d' = d/\vartheta, D' = 2D/\vartheta$ and $\vartheta = \lambda_W Z_C/\lambda_R f$.

From this equation it is apparent that the diffracted light is concentrated in three rectangular regions of the Fourier plane centred at points $(U-d',0)$, $(0,0)$ and $(U+d',0)$ of the plane U–V, as can be confirmed by observing figure 7. In figure 7 (*a*) a 3-D average intensity in the Fourier plane is represented. In figure 7 (*b*) and 7 (*c*) the average intensities through the coordinate axes U and V are depicted, respectively. The parameters selected are: $\lambda_R = 633\,\mathrm{nm}$, $\lambda_W = 514\,\mathrm{nm}$, $Z_C = 485\,\mathrm{nm}$, $f = 100\,\mathrm{mm}$, $d = 10\,\mathrm{mm}$, $D = 3.8\,\mathrm{mm}$, $e = 2$ and $\Delta X^{12} = -\Delta Y^{12} = 100\sqrt{2}\,\mu\mathrm{m}$.

To obtain the zero-order fringe visibility, we define the envelopes by using equation (26) as:

$$\langle I_f^0(U,V)\rangle_{\max} = 2CAI_R D^2\,\mathrm{trian}\left(\frac{2U}{D'}\right)\left\{e\,\mathrm{trian}\left(\frac{2V}{eD'}\right)+3\,\mathrm{trian}\left(\frac{2V}{D'}\right)\right\}, \quad (28)$$

$$\langle I_f^0(U,V)\rangle_{\min} = 2CAI_R D^2\,\mathrm{trian}\left(\frac{2U}{D'}\right)\left\{e\,\mathrm{trian}\left(\frac{2V}{eD'}\right)-\mathrm{trian}\left(\frac{2V}{D'}\right)\right\}, \quad (29)$$

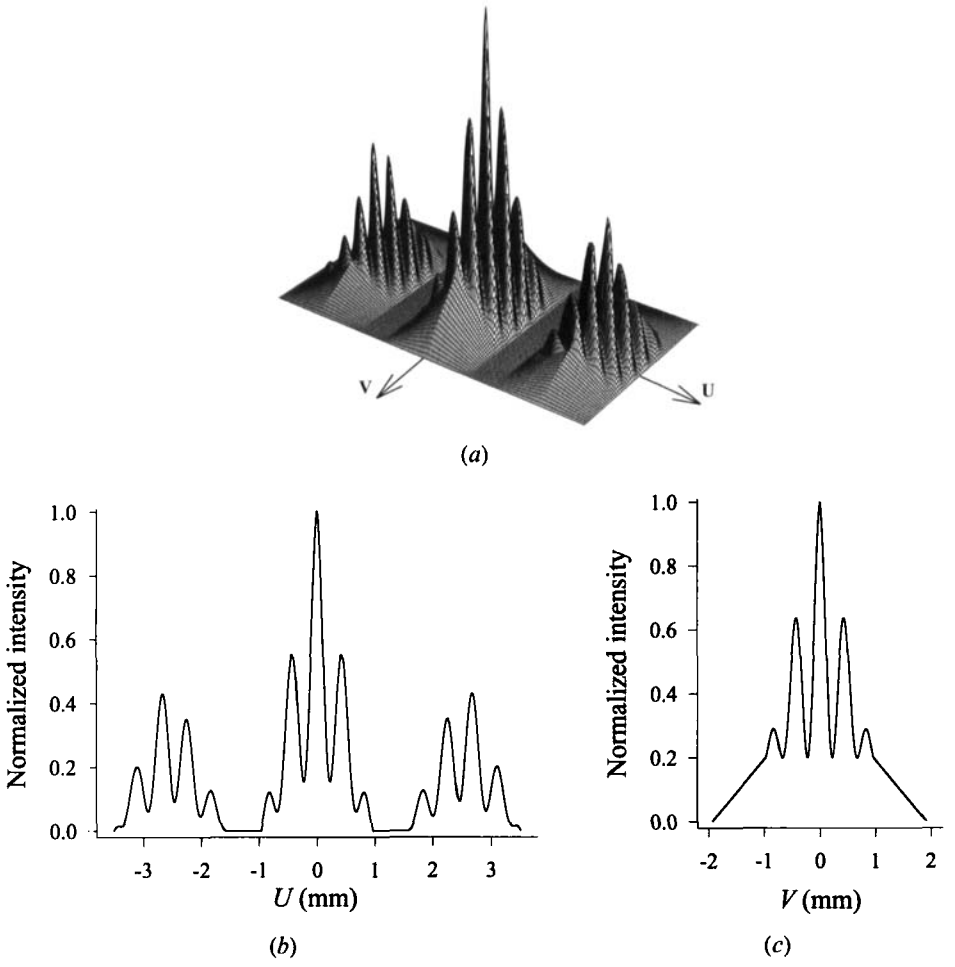

Figure 7. Theoretical simulation of the average intensity in the Fourier plane using a double exposure specklegram and the pupil aperture of figure 6: (*a*) 3D representation; (*b*) and (*c*) line profile along the U and V axis, respectively.

Then, the zero-order visibility results:

$$\mathbf{V}(V) = \frac{\langle I_f^0(U,V)\rangle_{\max} - \langle I_f^0(U,V)\rangle_{\min}}{\langle I_f^0(U,V)\rangle_{\max} + \langle I_f^0(U,V)\rangle_{\min}} = \frac{2\,\mathrm{trian}\left(\dfrac{2V}{D'}\right)}{\mathrm{trian}\left(\dfrac{2V}{D'}\right) + e\,\mathrm{trian}\left(\dfrac{2V}{eD'}\right)} \tag{30}$$

It should be pointed out that the lateral orders satisfy the same equation. This fact can be confirmed taking into account that: $\langle I_f^{\pm 1}(U,V)\rangle_{\max} = (1/2)\langle I_f^0(U \mp d', V)\rangle_{\max}$ and $\langle I_f^{\pm 1}(U,V)\rangle_{\min} = (1/2)\langle I_f^0(U \mp d', V)\rangle_{\min}$. Note that the visibility depends only on the V-coordinate associated to the pupil aperture change. The symmetry of the triangular functions implies that the visibility does not change when the coordinates change sign. At the origin $(U, V) = 0$ the

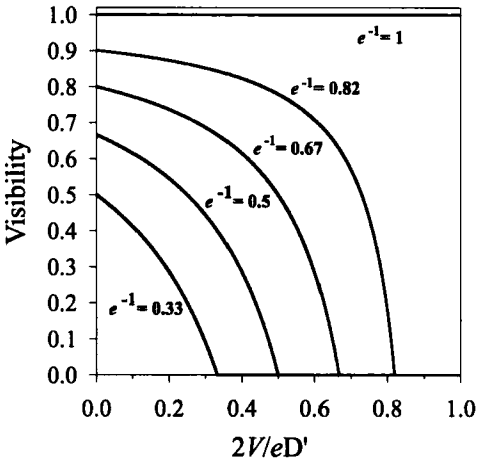

Figure 8. Fringe visibility curves for different values of the parameter e^{-1} obtained using scaled pupils aperture schematized in figure 6.

visibility reaches its maximum value $\mathbf{V}(0) = 2/(1+e)$. Figure 8 shows the visibility as a function of the parameter e.

Figure 9 displays the theoretical and experimental diffraction pattern $\langle I_f(U,V)\rangle$ corresponding to a double exposure specklegram by using a double aperture pupil with different scales between exposures. Note that the introduction of a horizontal and a vertical in-plane displacement between exposures is considered. The results in the first column are for a 100 μm horizontal in-plane displacement and those in the second column for a 100 μm vertical in-plane displacement. In both cases, the parameters employed are: $\lambda_W = \lambda_R = 633$ nm, $Z_0 = 135$ mm, $Z_C = 485$ mm, $f = 100$ mm, $d = 10$ mm, $D = 3.8$ mm and $e = 2$. The line profile of one of the lateral diffraction orders is shown along with each diffraction pattern. The profile was taken along the interferometric fringes that modulate the centre of the corresponding lateral diffraction order. The results of the first row are simulated using equations (25), (26) and (27) and the selected parameter values. The results depicted in the second row are obtained experimentally, following the procedure as detailed in section 3.1. Note that the images of the first row correspond to the smoothed intensity functions and, in consequence, the high frequency modulation associated to the speckles is not present. Nevertheless, the speckle appearing in the second file corresponds to the experimental intensity distribution without any averaging. The profiles corresponding to the experimental results of the second row are smoothed by applying a low-pass filter to the respective images. From the results of figure 9 it is apparent that the use of multiple apertures with different scale factors in each direction implies that fringes visibility depends on the scale ratio. In particular as predicted in equation (30), fringe visibility decreases along the V axis, from the centre to the outsides.

4. Conclusions

In this paper, the effect of modifying the aperture pupil scale between exposures in speckle photography is analysed. In particular, the Young fringe

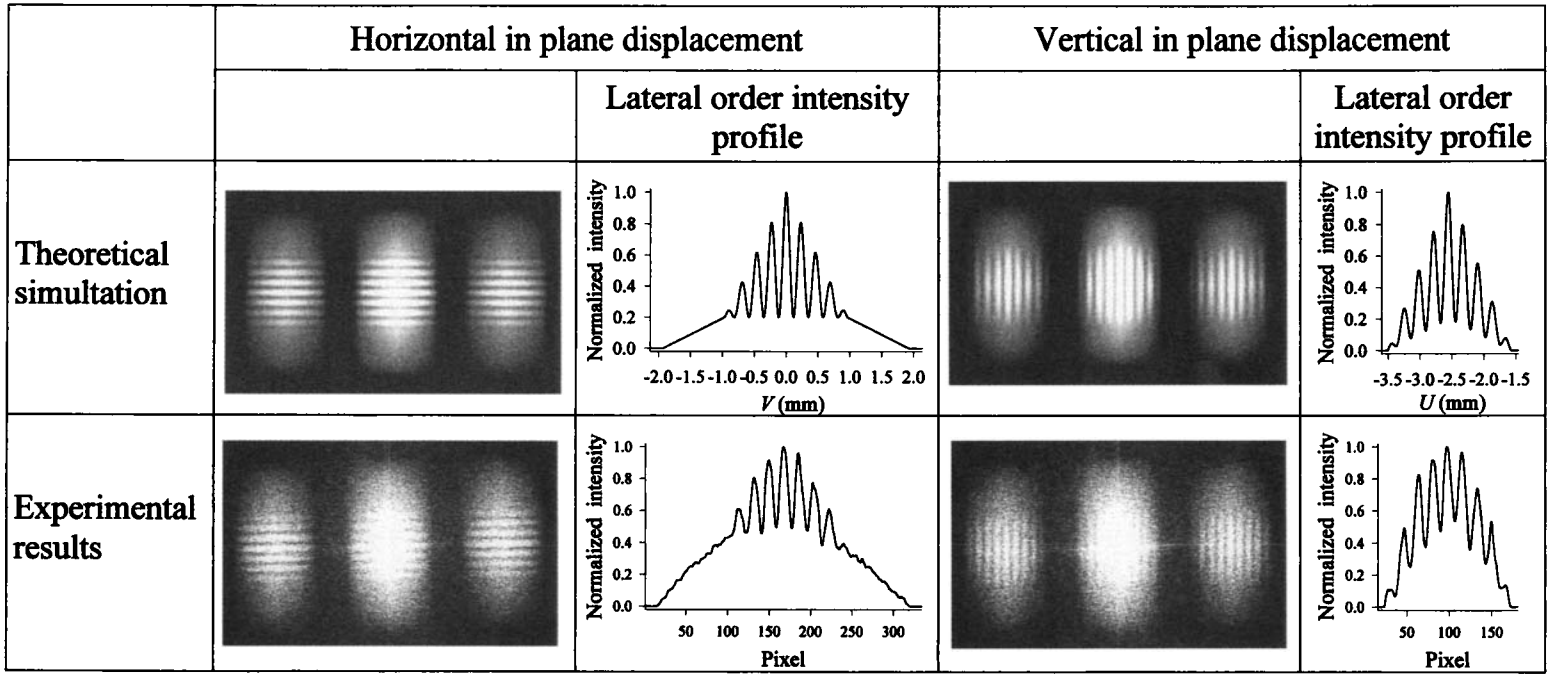

Figure 9. The first row shows the theoretical smoothed density plot of the average intensity in the Fourier plane and the corresponding profile along the direction perpendicular to the fringes using the pupil aperture of figure 6 and with a 100 μm vertical and horizontal in-plane displacement. The second row shows the experimental results corresponding to the same situation described above.

visibility produced by double exposure specklegrams is investigated when the plane displacement between exposures is implemented and pupils with one or multiple apertures are used. Then, by employing a different scaled pupil in each exposure, different speckle patterns are registered in each exposure. It was established that the general expression for the average intensity of the spectra can be formulated in terms of the pupil functions employed and the diffuser displacement.

The average intensity in the Fourier plane has two terms. One term takes into account the superposition of the smoothed diffraction halos corresponding to each exposure. The second term describes the correlation fringes formation in the Fourier plane. It is established that each pupil pair can be associated with an individual contribution to fringe formation. Besides, the fringes are obtained in the common region of the diffraction patterns belonging to each pupil. Also, it is demonstrated that this region depends on the common transmission area of the pupils.

It should be mentioned that the scaled aperture analysis deepens the speckle decorrelation introduced by object displacement and the changes in diffuser illumination conditions studied elsewhere [5, 7, 8].

When pupils with one circular aperture scaled between expositions are used, the fringe visibility reaches its maximum value at the centre of the common diffraction region and it is null outside the non-common diffraction halos. The fringe visibility decreases gradually in between. It was shown that the fringes visibility depends on the scale ratio.

To generalize our treatment, we consider the use of multiple apertures with different scale factors in each direction. Also it is apparent that fringes visibility depends on the scale ratio.

Acknowledgments

This research was performed under the auspicious of CONICET, CICPBA, Faculty of Engineering of the National University of La Plata (Argentina). M. Tebaldi acknowledges CONICET (Argentina).

References

[1] Burch, J. M., and Tokarski, M. J., 1968, *Optica Acta*, **15**, 101–111.
[2] Archbold, E., Burch, J. M., and Ennos, A. E., 1970, *Optica Acta*, **17**, 883.
[3] Archbold, E., Burch, J. M., and Ennos, A. E., 1970, *Optica Acta*, **19**, 253.
[4] Chiang, F. D., and Khetan, R. P., 1979, *Appl. Optics*, **18**, 2175–2186.
[5] Yamaguchi, I., 1985, Fringe formation in deformation and vibration measurements using laser light. In *Progress in Optics*, Vol. XXII, edited by E. Wolf (North-Holland: Elsevier Science Publishers B.V.), pp. 271–339.
[6] Rastogi, P. K., 1993, Techniques of displacement and deformation measurements in speckle metrology. In *Speckle Metrology*, edited by R. Sirohi (New York: Marcel Dekker, Inc.), pp. 41–98.
[7] Li, D. W., Chen, J. B., and Chiang, F. P., 1985, *J. Opt. Soc. Amer.*, **A2**, 657–666.
[8] Sjödal, M., 1995, *Appl. Optics*, **34**, 7798–8010.
[9] Kaufmann, G. H., 1981, *Appl. Optics*, **20**, 4277–4280.
[10] Meynart, R., 1984, *Appl. Optics*, **23**, 2235–2236.
[11] Angel Toro, L., Tebaldi, M., Bolognini, N., and Trivi, M., 2000, *J. Opt. Soc. Amer.*, **A17**, 107–119.

[12] GOODMAN, J. W., 1975, Statistical properties of laser speckle patterns. In *Laser Speckle and Related Phenomena*, edited by J. C. DAINTY (New York: Springer-Verlag), pp. 11–76.
[13] NAKAGAWA, K., TAKATSUJI, T., and MINEMOTO, T., 1990, *Opt. Commun.*, **76,** 206–212.
[14] FRANÇON, M., 1979, *Laser Speckle and Applications in Optics* (New York: Academic Press), p. 16.